Multi-vehicle dynamics and control for aerial recovery of micro air vehicles

Liang Sun

Department of Electrical and Computer Engineering,
Brigham Young University,
Provo, UT, USA
E-mail: sun.liang@byu.edu

Mark B. Colton* and Daniel C. Carlson

Department of Mechanical Engineering,
Brigham Young University,
Provo, UT, USA
E-mail: colton@byu.edu
E-mail: danielcarlson@byu.edu
*Corresponding author

Randal W. Beard

Department of Electrical and Computer Engineering,
Brigham Young University,
Provo, UT, USA
E-mail: beard@byu.edu

Abstract Aerial recovery of micro air vehicles (MAVs) presents a challenging problem in multi-vehicle dynamics and control. This paper presents a method for recovering MAVs in flight using a mothership and towed drogue, in which the mothership executes an orbit that places the drogue in a stable, slower orbit that can be tracked by a MAV. A method for modeling the dynamics of the mothership-cable-drogue system, based on Gauss's principle, is presented. The differential flatness property of the system is exploited to calculate mothership trajectories from desired drogue orbits, and a backstepping controller is proposed that enables accurate mothership trajectory tracking. A drag-based controller for the drogue is also described. Methods to enable the MAV to estimate and track the drogue orbit are discussed. The modeling and control methods are illustrated through simulation and flight results.

Keywords: unmanned air vehicles; micro air vehicles; multi-vehicle systems; aerial recovery; towed cable systems

Reference to this paper should be made as follows: Sun, L., Colton, M.B., Carlson, D.C. and Beard, R.W. 'Multi-vehicle dynamics and control for aerial recovery of micro air vehicles', *Int. J. Vehicle Autonomous Systems*, Vol. x, No. x, pp.xxx–xxx.

Copyright © 2009 Inderscience Enterprises Ltd.

Biographical notes: Liang Sun is a Ph.D. student in the Department of Electrical and Computer Engineering at Brigham Young University. He received his B.S. and M.S. degrees from Beihang University, China, in 2004 and 2007, respectively. His research is in the field of unmanned air vehicles, with specific emphasis on dynamic modeling and control.

Mark B. Colton is an assistant professor in the Department of Mechanical Engineering at Brigham Young University since 2006. He received the B.S. degree in 1997, the M.S. degree in 2001, and the Ph.D. degree in 2006, all from the University of Utah. His research interests include unmanned air vehicles, haptic interfaces, and socially assistive robotics.

Daniel C. Carlson is an M.S. student in the Department of Mechanical Engineering at Brigham Young University. He received his B.S. degree in Mechanical Engineering from Brigham Young University in 2008. His research is in the field of unmanned air vehicles, with specific emphasis on orbit estimation and tracking.

Randal W. Beard received the B.S. degree in electrical engineering from the University of Utah, Salt Lake City in 1991, the M.S. degree in electrical engineering in 1993, the M.S. degree in mathematics in 1994, and the Ph.D. degree in electrical engineering in 1995, all from Rensselaer Polytechnic Institute, Troy, NY. Since 1996, he has been with the Electrical and Computer Engineering Department at Brigham Young University, Provo, UT, where he is currently a professor. In 1997 and 1998, he was a Summer Faculty Fellow at the Jet Propulsion Laboratory, California Institute of Technology, Pasadena, CA. In 2006 and 2007 he was a visiting research fellow at the Air Force Research Laboratory, Munitions Directorate, Eglin AFB, FL. His primary research focus is autonomous control of miniature air vehicles and multivehicle coordination and control.

1 Introduction

In recent years, the use of unmanned air systems (UASs) has increased dramatically in both military and civilian fields, with applications ranging from intelligence, surveillance, and reconnaissance (ISR) to wilderness search and rescue. In most current applications large and costly UASs, such as the Predator and the Global Hawk, are used for their high-altitude and long-endurance capabilities. However, as the potential applications for UAS technologies increase, the emphasis on smaller platforms is also growing. Micro air vehicles (MAVs), with wingspans typically less than 15 inches, have the potential to open new application areas and broaden the availability of UAS technology. The potential of MAVs is driven primarily by their relatively low cost, superior portability, and, in some cases, improved stealth. The net result is that MAVs may be used in greater numbers and by personnel who otherwise would not have access to UAS technology. In certain applications, the ability of individual personnel (such as soldiers, rescue workers, or scientists) to carry and deploy MAVs in situ (on the battlefield, in a disaster area, or around volcanoes) would be of considerable benefit.

The ability to deploy MAVs locally and in large numbers opens many opportunities, but recovery of MAVs is problematic in certain scenarios. For instance, if a soldier deploys a backpackable MAV on the battlefield to gather time-critical ISR information, it is undesirable for the MAV to return to the soldier because this could disclose his/her location to the enemy. Additionally, if a large mothership deploys multiple MAVs in a remote location for ISR, wildfire monitoring, or other surveillance, the MAVs may not have sufficient range to return to a distant base. Similarly, in disaster areas that are too remote or dangerous, MAV search or monitoring platforms may not be recovered by ground personnel.

One solution to this problem is to use a mothership as an aerial recovery platform for MAVs. The primary challenge with this approach is the high speed of the mothership relative to the MAV, which makes direct MAV/mothership rendezvous and capture impractical. Furthermore, aerial recovery must be highly accurate, as the rendezvous and capture must be coordinated in both time and space. The approach taken in the present work is to employ a capture device (drogue) that is towed by a larger mothership, as shown in Figure 1. In this method, the mothership enters an orbit designed to cause the towed drogue to execute an orbit of smaller radius and lower speed (less than the nominal speed of the MAV). The MAV then enters the drogue orbit at its nominal airspeed and overtakes the drogue with a relatively slow closing speed. In the terminal stages of rendezvous and capture, a vision-based homing algorithm, such as proportional navigation (PRONAV), is used to close the gap between MAV and drogue (Zarchan, 1990; Siouris, 2004).

The aerial recovery approach described in this paper is therefore a challenging problem in multi-vehicle modeling and control involving three vehicles: MAV, mothership, and drogue. This paper focuses on novel contributions to four key elements of the aerial recovery problem:

1. *Modeling of mothership-cable-drogue system* (Section 2). We present an accurate forward dynamics model to predict trajectories of a passive drogue for given trajectories of the mothership. This N-link model, based on Gauss's principle, enables simulation and testing of the interactions between the mothership and a passive drogue.

2. *Mothership path planning and control* (Section 3). For the case of passive drogues, which can only be controlled indirectly via the mothership, it is necessary to have a method to calculate the orbit that the mothership must execute to place the drogue in an orbit suitable for aerial recovery of a slower MAV. An inverse dynamics model, based on the principal of differential flatness, is developed to enable calculation of the required mothership orbit from a specified drogue orbit. A Lyapunov-based backstepping control law is also developed to ensure accurate tracking of the orbit by the mothership.

3. *Active drogue control for improved orbit tracking* (Section 4). To complement the indirect control of the drogue (via the mothership), we develop an active drogue control approach based on modulation of the drogue drag coefficient. We show that the drogue orbit radius may be controlled by changing the drag of the drogue. This approach will allow more accurate orbit tracking to facilitate the final MAV/drogue rendezvous.

4. *MAV orbit estimation and tracking* (Sections 5 and 6). After the mothership and active or passive drogue establish a suitable orbit, the MAV must enter the drogue orbit and approach the drogue for capture of the MAV to occur. We develop methods that enable the MAV to estimate the drogue orbit from GPS data, and track the orbit in preparation for final rendezvous. Future work will address the problem of final approach and docking, including hardware design and PRONAV algorithms.

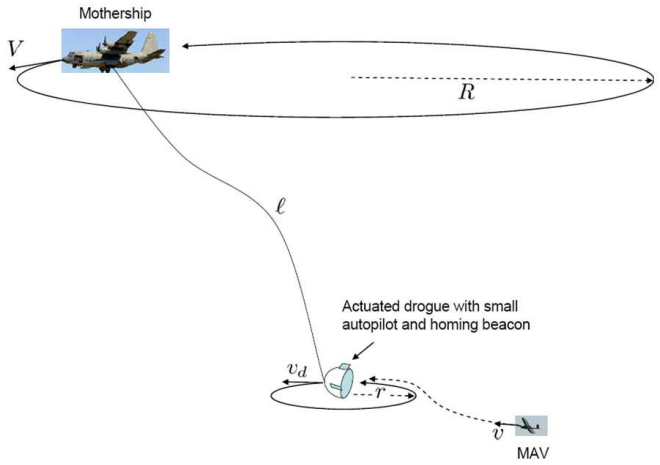

Figure 1 Basic aerial recovery concept. The mothership recovers a MAV by towing a drogue that is actuated and can maneuver and communicate with the MAV to facilitate successful capture.

As outlined, the primary purpose of this work is to model the dynamics of mothership-drogue-MAV interactions, develop control laws to enable orbit generation and tracking, and validate these concepts primarily through simulation. Initial experimental results are provided for the orbit-generation component of aerial recovery; future work will involve extensive flight tests to validate and refine the remaining components.

Our approach is motivated by previous work on the dynamics of towed cable systems. Skop and Choo (1971) show that if a towplane maintains a constant-angular-rate orbit of radius R, and the drogue has sufficient aerodynamic drag, then the drogue will execute a stable orbit of radius $r \ll R$. Furthermore, since the angular rates of the towplane and the drogue must be the same, the speed of the drogue will be less than the speed of the towplane. Murray (1996) designs a path planning algorithm for the towplane with the objective of minimizing the orbit radius of the drogue. In more recent work, Williams and Trivailo (2007a) and Williams and Trivailo (2007b) give a detailed description of the dynamics of circularly towed drogues and design strategies for moving from one orbit configuration to another. The objective in Williams and Trivailo (2007a) and Williams and Trivailo (2007b) is precision pickup and delivery of payloads on the ground by a fixed-wing aircraft. More recently, Williams and Ockels (2009) employed this approach to the problem of lifting payloads using multiple fixed-wing aircraft. Their

work proved the concept's feasibility and studied the equilibria and stability of such systems. The focus in Murray (1996), Williams and Trivailo (2007a), Williams and Trivailo (2007b), and Williams and Ockels (2009) is on minimizing the orbit radius of the drogue. For aerial recovery of MAVs, we take a different approach to the problem. As shown in Figure 1, rather than attempting to minimize the radius of the orbit of the drogue, our objective will be to place the drogue in a stable orbit whose radius r is greater than the minimum turning radius of the MAV.

2 Mathematical model of cable-drogue system

Mathematical models of cable-drogue or towed-cable systems are established in the literature for both air and underwater environments. Several approaches to modeling cable dynamics have been described. Choo and Casarella (1973) compare various methods and describe the relative strengths and limitations of each. They conclude that, despite the heavy computational workload required for implementation, the finite element, or lumped mass technique is the most versatile of the methods studied. Using the finite element approach, the cable in the cable-drogue system may be modeled as a finite number of rigid links of uniform length, and the drogue as a point mass, which is the last joint of the cable. Figure 2 depicts this approach, with the cable modeled as N rigid links.

The approaches to modeling the cable dynamics described in the literature require that the internal and external forces are described explicitly. Murray (1996) develops towed-cable dynamics based on the Lagrange approach, which requires an explicit derivation of the tension in the cable. Cochran et al. (1992) develop an approach to eliminating constraint forces in the cable that maintains constant link lengths through a change of variables. Chin and Connell (2000) apply partial differential equations to model the cable-body system and solve them using the finite difference method. Turkyilmaz and Egeland (2001) develop a two-dimensional dynamic model for a towed cable for seismic survey studies. Williams and Trivailo (2007a) derives the equations of motion of the system by introducing cable attitude angles. These methods result in dynamic model equations that are complicated and difficult to use for the purposes of simulation and control design.

Most of the methods reported in the literature use techniques that model the cable as a series of $N < \infty$ rigid links with lumped masses at the joints. As recommended in Choo and Casarella (1973), we also followed this approach. However, most researchers develop models based on Euler-Lagrange equations, which do not scale well to a large number of links. As an alternative, we develop the mathematical model of cable-drogue systems using Gauss's Principle, as described in the work of Udwadia and Kalaba (1996). A similar approach was used in the context of path planning for UAVs in McLain and Beard (2000). As will be demonstrated in the next section, this method is well-suited to problems with complex internal forces, as seen in mothership-cable-drogue interactions. Rather than computing internal forces between cable links directly, the kinematic constraints are employed.

2.1 Gauss's Principle

Consider a system of n particles of mass $m_1, m_2, ..., m_n$. Let the vector $\mathbf{p}_i = (x_i, y_i, z_i)^T$ represent the position of the i^{th} particle of this system in a rectangular

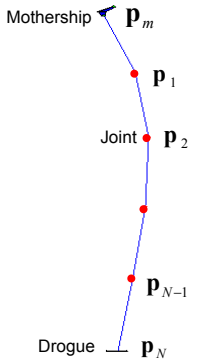

Figure 2 N-link lumped mass representation of cable-drogue system

inertial reference frame (Udwadia and Kalaba, 1996). We assume that the i^{th} particle is subjected to a given impressed force $\mathbf{F}_i(t)$, so that its acceleration without constraints would be given by the vector $\mathbf{a}_i = \mathbf{F}_i(t)/m_i$. The three components of the vector $\mathbf{a}_i$ correspond to the accelerations of the i^{th} particle driven by $\mathbf{F}_i$ in the three mutually perpendicular coordinate directions. Thus the equations of motion without constraints on the particles of the system can be written as

$$\mathbf{M}\mathbf{a}(t) = \mathbf{F}(\mathbf{x}(t), \dot{\mathbf{x}}(t), t), \tag{1}$$

where

$$\begin{aligned}
\mathbf{F}(t) &= (\mathbf{F}_1^T, \mathbf{F}_2^T, ..., \mathbf{F}_n^T)^T \\
\mathbf{a}(t) &= (\mathbf{a}_1^T, \mathbf{a}_2^T, ..., \mathbf{a}_n^T)^T \\
\mathbf{x}(t) &= (\mathbf{p}_1^T, \mathbf{p}_2^T, ..., \mathbf{p}_n^T)^T \\
\mathbf{M} &= \mathrm{Diag}(m_1, m_1, m_1, m_2, ..., m_n, m_n, m_n).
\end{aligned}$$

In the presence of constraints, the acceleration of each particle at time t will differ from $\mathbf{a}(t)$. We denote this constrained acceleration by the $3n$-vector $\ddot{\mathbf{x}}(t) = (\ddot{\mathbf{p}}_1^T, \ddot{\mathbf{p}}_2^T, ..., \ddot{\mathbf{p}}_n^T)^T$. Gauss's principle asserts that, among all the accelerations that the system can have at time t that are compatible with the constraints, the accelerations that actually occur are those that minimize

$$G(\ddot{\mathbf{x}}) = (\ddot{\mathbf{x}} - \mathbf{a})^T \mathbf{M} (\ddot{\mathbf{x}} - \mathbf{a}) = (\mathbf{M}^{1/2}\ddot{\mathbf{x}} - \mathbf{M}^{1/2}\mathbf{a})^T (\mathbf{M}^{1/2}\ddot{\mathbf{x}} - \mathbf{M}^{1/2}\mathbf{a}). \tag{2}$$

Assuming that the m constraints can be expressed as linear equality relations between the accelerations of the particles of the system, the constraints will always be of the standard form

$$\mathbf{A}(\dot{\mathbf{x}}, \mathbf{x}, t)\ddot{\mathbf{x}} = \mathbf{b}(\dot{\mathbf{x}}, \mathbf{x}, t), \tag{3}$$

where the matrix $\mathbf{A}$ is m by $3n$ and the vector $\mathbf{b}$ is an m-vector.

Minimizing (2) subject to the constraint (3) implies that at each instant of time t, the actual acceleration of the system of n particles is given by

$$\ddot{\mathbf{x}} = \mathbf{a} + \mathbf{M}^{-1/2}(\mathbf{A}\mathbf{M}^{-1/2})^+(\mathbf{b} - \mathbf{A}\mathbf{a}), \tag{4}$$

where $(\cdot)^+$ is the unique Moore-Penrose inverse (Udwadia and Kalaba, 1996).

2.2 Dynamic equations of cable-drogue systems using Gauss's Principle

Figure 2 depicts the cable-drogue system with the cable modeled as N rigid links. The forces acting on each link are lumped and applied at the joints, and the drogue is the last joint of the cable. Let $\mathbf{p}_i = (x_i, y_i, z_i)^T \in \mathbf{R}^3, i = 1, 2, ..., N$ be the location of the ith link. The position of the towplane or mothership is $\mathbf{p}_m = (x_m, y_m, z_m)^T \in \mathbf{R}^3$. If the point masses associated with each link are unconstrained, then the dynamic equations describing their motion are

$$\begin{aligned} \ddot{\mathbf{p}}_i &= \mathbf{a}_i, \quad i = 1, 2, ..., N, \\ \ddot{\mathbf{p}}_m &= \mathbf{a}_m, \end{aligned}$$

where $\mathbf{a}_i, i = 1, 2, ..., N,$ and $\mathbf{a}_m \in \mathbf{R}^3$ are the unconstrained accelerations driven by the applied forces in three dimensions. Alternatively, defining $\mathbf{x} = (\mathbf{p}_1^T, \mathbf{p}_2^T, \cdots, \mathbf{p}_N^T)^T$ and $\mathbf{a} = (\mathbf{a}_1^T, \mathbf{a}_2^T, \cdots, \mathbf{a}_N^T)^T$ gives

$$\ddot{\mathbf{x}} = \mathbf{a}. \tag{5}$$

However, the motion of the point masses associated with each link are constrained by the relationship

$$\begin{aligned} \|\mathbf{p}_1 - \mathbf{p}_m\|^2 &= l^2, \\ \|\mathbf{p}_{i+1} - \mathbf{p}_i\|^2 &= l^2, \ i = 1, 2, ..., N-1, \end{aligned}$$

where L is the cable length and $l = L/N$ is the length of each link. These position constraints may also be expressed in matrix form as

$$\phi(\mathbf{x}, \mathbf{p}_m) \triangleq \begin{pmatrix} \|\mathbf{p}_1 - \mathbf{p}_m\|^2 - l^2 \\ \|\mathbf{p}_2 - \mathbf{p}_1\|^2 - l^2 \\ \vdots \\ \|\mathbf{p}_N - \mathbf{p}_{N-1}\|^2 - l^2 \end{pmatrix} = 0. \tag{6}$$

Differentiating (6) with respect to time results in the velocity constraint

$$\psi(\mathbf{x}, \mathbf{p}_m) \triangleq \begin{pmatrix} (\mathbf{p}_1 - \mathbf{p}_m)^T(\dot{\mathbf{p}}_1 - \dot{\mathbf{p}}_m) \\ (\mathbf{p}_2 - \mathbf{p}_1)^T(\dot{\mathbf{p}}_2 - \dot{\mathbf{p}}_1) \\ \vdots \\ (\mathbf{p}_N - \mathbf{p}_{N-1})^T(\dot{\mathbf{p}}_N - \dot{\mathbf{p}}_{N-1}) \end{pmatrix} = 0. \tag{7}$$

Assuming that the motion of the mothership $(\mathbf{p}_m, \dot{\mathbf{p}}_m, \ddot{\mathbf{p}}_m)$ is known, the acceleration constraints can be written in matrix form as

$$\mathbf{A}(\mathbf{x})\ddot{\mathbf{x}} = \mathbf{b}(\dot{\mathbf{x}}, \dot{\mathbf{p}}_m, \ddot{\mathbf{p}}_m), \tag{8}$$

where

$$\mathbf{A} = \begin{pmatrix} (\mathbf{p}_1 - \mathbf{p}_m)^T & 0 & \cdots & 0 \\ -(\mathbf{p}_2 - \mathbf{p}_1)^T & (\mathbf{p}_2 - \mathbf{p}_1)^T & \cdots & 0 \\ \vdots & \ddots & \ddots & \vdots \\ 0 & \cdots & -(\mathbf{p}_N - \mathbf{p}_{N-1})^T & (\mathbf{p}_N - \mathbf{p}_{N-1})^T \end{pmatrix},$$

$$\mathbf{b} = -\begin{pmatrix} \|\dot{\mathbf{p}}_1 - \dot{\mathbf{p}}_m\|^2 \\ \|\dot{\mathbf{p}}_2 - \dot{\mathbf{p}}_1\|^2 \\ \vdots \\ \|\dot{\mathbf{p}}_N - \dot{\mathbf{p}}_{N-1}\|^2 \end{pmatrix} + \begin{pmatrix} (\mathbf{p}_1 - \mathbf{p}_m)^T \ddot{\mathbf{p}}_m \\ 0 \\ \vdots \\ 0 \end{pmatrix}.$$

Based on Gauss's principle, the actual acceleration of the cable-drogue system (5) subject to the constraints (8) is given by (4). The initial conditions for the system must be chosen such that both $\phi(\mathbf{x}, \mathbf{p}_m) = 0$ and $\psi(\mathbf{x}, \mathbf{p}_m) = 0$.

As indicated by McLain and Beard (2000), one of the drawbacks of this method is that while solving (4), numerical errors may cause the constraints $\phi(\mathbf{x}, \mathbf{p}_m)$ and $\psi(\mathbf{x}, \mathbf{p}_m)$ to drift from zero. When this happens, Equation (4) no longer represents the physical dynamics of the cable. That is to say, no mechanism serves to drive the constraints back to zero. To mitigate this problem, Equation (4) is modified as (McLain and Beard, 2000)

$$\ddot{\mathbf{x}} = \mathbf{a} + \mathbf{M}^{-1/2}(\mathbf{A}\mathbf{M}^{-1/2})^{+}(\mathbf{b} - \mathbf{A}\mathbf{a}) - \gamma_1(\frac{\partial \phi}{\partial \mathbf{x}})^T \phi - \gamma_2(\frac{\partial \psi}{\partial \mathbf{x}})^T \psi,$$

where γ_1 and γ_2 are positive constants that are tuned through simulation to give satisfactory convergence for the selected link lengths of the cable model. For example, for a 1000 meter cable modeled as 10 links (100 meters per link), γ_1 and γ_2 were given the values of 0.05 and 0.002, respectively. The additional two terms cause the ODE solution to decrease the gradient of the constraints until they are not violated. Selecting γ_1 and γ_2 properly guarantees that the modified equation approximately represents the dynamics of the constrained physical system. The mass matrix $\mathbf{M} = \text{Diag}(m_l, m_l, ..., m_l, m_d, m_d, m_d) \in \mathbf{R}^{3N \times 3N}$, where m_c is the total mass of the cable, $m_l = m_c/N$ is the mass of each link, and m_d is the mass of the drogue.

2.3 Dynamic model simulation results

The model presented in the previous section enables simulation of the mothership-drogue dynamics. The simulation architecture used in this and subsequent simulations is shown in Figure 3. In the simulations presented in this paper wind is not considered, and the air density does not vary as a function of altitude. Future work will address these issues.

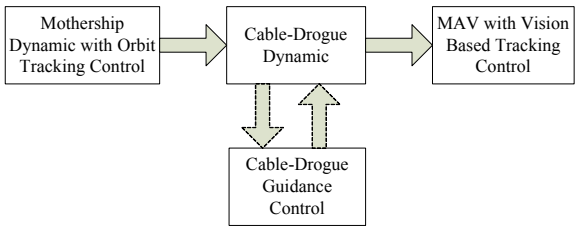

Figure 3 Simulation system. The mothership flies in a constant-radius orbit and does not feel tension from cable-drogue system. Passive and active drogue modes are selectable by the user.

Key simulation parameters are shown in Table 1 for a simulation in which the mothership follows a fixed circular orbit at a constant velocity while towing a passive drogue. Figure 4 shows that the steady radius of the drogue oscillates between 115 and 119 m. The steady state drogue velocity is approximately 19.5 m/s, which is larger than the velocity of the MAV. Therefore, for the conditions considered, the MAV cannot rendezvous with the drogue. Figure 5 shows the two-dimensional top-down view and three-dimensional view of the simulated system. The cable bows outward under the effect of the aerodynamic drag.

Table 1 Parameters for simulation of passive and active drogue control

Mothership	Airspeed	Altitude	Orbit Radius	
	50 m/s	1000 m	300 m	
Cable	Links	Length	Diameter	Mass
	10	900 m	0.01 m	0.01 kg
MAV	Airspeed			
	16.67 m/s			

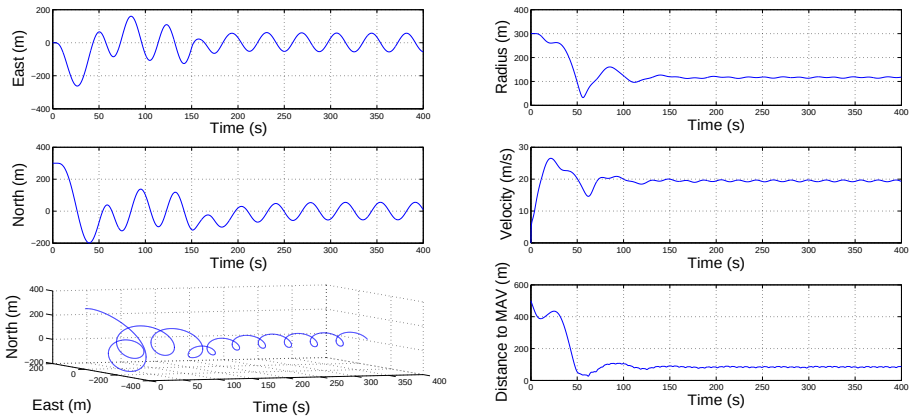

Figure 4 Simulation of passive drogue motion in response to a circular mothership orbit. Shows north and east motion of the drogue (left) and the radius, velocity and distance to the MAV of the drogue (right). Steady state is reached after approximately 150 s.

3 Mothership path planning and control

The previous section described methods for deriving the forward dynamic equations for the mothership-cable-drogue system, which enables us to calculate the motion of the drogue for a given motion of the mothership. In this section we develop methods for the inverse problem: calculating the required mothership trajectory to achieve a desired drogue trajectory. We also develop a Lyapunov-based

backstepping algorithm to cause the mothership to track the desired orbit accurately, with the goal of achieving accurate drogue orbits. We assume that the drogue is passive, i.e., it is only controlled indirectly via the mothership and cable, and that it is instrumented with a small autopilot and therefore has access to its own acceleration, angular rates, airspeed, and GPS location. Under these assumptions, the basic idea is to control the motion of the mothership so that the drogue enters a specified stable orbit whose radius r is greater than the minimum turning radius of the MAV, at an airspeed that is slightly below the nominal airspeed of the MAV.

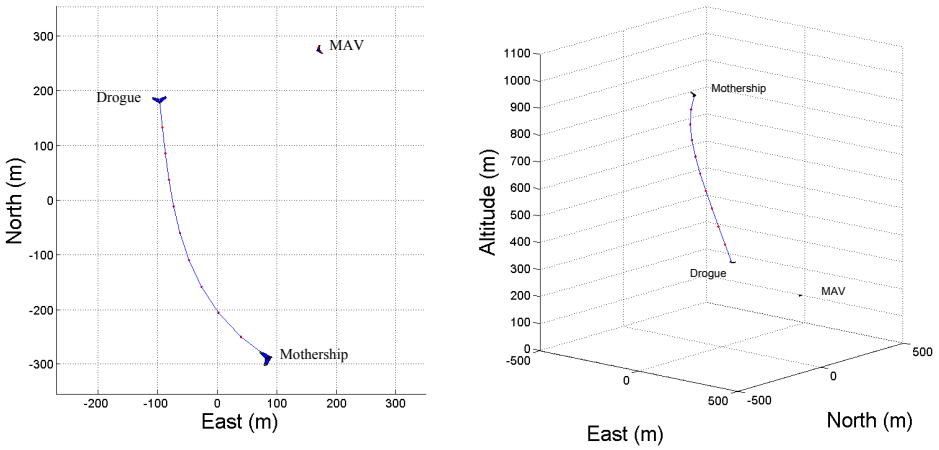

Figure 5 Top-down and 3D views of the simulated mothership and passive drogue. The dots on the cable represent joints.

In recent decades, control strategies to address related problems have appeared in the literature. The concept of differential flatness of the system is exploited in Murray (1996) to plan towplane paths that minimize the motion of the drogue. This work shows that the trajectory of the towplane is uniquely prescribed by the motion of the drogue. Unfortunately, the algorithm as presented in Murray (1996) has numerical stability issues. In Williams and Trivailo (2007a), sequential quadratic programming is used to plan open-loop trajectories for the towplane. Williams and Trivailo (2007b) addresses the problem of entering and exiting the orbit with the cable deployed, and open-loop strategies are derived that minimize the tension on the cable and the drogue. Williams and Trivailo (2007b) also addresses the problem of deploying the cable from the towplane using a winch after the towplane is in its orbit. The majority of prior work in this area is related to the dynamics and stability of the drogue; few studies have explored specific strategies for accurate control of the mothership-cable-drogue system.

3.1 Mothership orbit calculation using differential flatness

The concept of differential flatness has been proved to be useful in the design of advanced control and supervision schemes for nonlinear systems. Fliess et al. (1995)

introduces the measure to define flat systems and apply the differential flatness theory to vertical take-off aircraft and articulated ground vehicles. Lu et al. (2005, 2007, 2008) show the application of differential flatness in vehicle trajectory tracking problems using neural networks to implement dynamic inversion. We make use of this property to calculate the inverse dynamics relating a desired drogue orbit to the required orbit of the mothership.

Definition The system $\dot{\mathbf{x}} = \mathbf{f}(\mathbf{x}, \mathbf{u}, t)$ where the states $\mathbf{x} \in \mathbb{R}^n$ and the inputs $\mathbf{u} \in \mathbb{R}^m$, is differentially flat if we can find a set of variables $\mathbf{y} \in \mathbb{R}^m$ called flat outputs and integers r and q such that

$$\begin{aligned}
\mathbf{y} &= \mathbf{h}(\mathbf{x}, \mathbf{u}, \dot{\mathbf{u}}, \ddot{\mathbf{u}}, \cdots, \mathbf{u}^{(r)}) \\
\mathbf{x} &= \mathbf{h}_1(\mathbf{y}, \dot{\mathbf{y}}, \ddot{\mathbf{y}}, \cdots, \mathbf{y}^{(q)}) \\
\mathbf{u} &= \mathbf{h}_2(\mathbf{y}, \dot{\mathbf{y}}, \ddot{\mathbf{y}}, \cdots, \mathbf{y}^{(q+1)})
\end{aligned}$$

that satisfy the system state equations.

Assuming that the only forces on the drogue are aerodynamic forces, gravity, and tension forces from the cable, the cable-drogue system is differentially flat using the trajectory of the drogue as a flat output. Therefore, specifying the desired trajectory of the drogue will dictate the required trajectory for each cable link, and, consequently, for the mothership.

Suppose that the trajectory of the drogue is C^∞, i.e., it has derivatives of all orders. We can then compute the tension components in the N^{th} link of the cable (at the end attached to the drogue) from

$$\begin{aligned}
T_N^x &= m_N \ddot{x}_N - F_N^x \\
T_N^y &= m_N \ddot{y}_N - F_N^y \\
T_N^z &= m_N \ddot{z}_N - F_N^z + m_N g,
\end{aligned}$$

where F_N^x, F_N^y, F_N^z are the aerodynamic forces acting on the drogue, expressed in the inertial frame. Assuming the length of each link is a constant $l = L/N$, the location of the $(j-1)^{th}$ mass point (located at the $(j-1)^{th}$ joint) is related to the j^{th} mass point using

$$\begin{aligned}
x_{j-1} &= x_j + l \frac{T_j^x}{\|\mathbf{T}_j\|} \\
y_{j-1} &= y_j + l \frac{T_j^y}{\|\mathbf{T}_j\|} \\
z_{j-1} &= z_j + l \frac{T_j^z}{\|\mathbf{T}_j\|} \\
j &= 2, 3, \cdots, N,
\end{aligned}$$

where $\|\cdot\|$ denotes the Euclidean norm. Consequently, the forces on the $(j-1)^{th}$ mass point can be calculated by

$$T_{j-1}^x = m_{j-1} \ddot{x}_{j-1} - F_{j-1}^x + T_j^x$$

$$
\begin{aligned}
T^y_{j-1} &= m_{j-1}\ddot{y}_{j-1} - F^y_{j-1} + T^y_j \\
T^z_{j-1} &= m_{j-1}\ddot{z}_{j-1} - F^z_{j-1} + T^z_j + m_{j-1}g \\
j &= 2, 3, \cdots, N, .
\end{aligned}
$$

At each time step, these equations are applied recursively to each link of the cable until the trajectory of the mothership is calculated.

3.2 Mothership trajectory tracking using Lyapunov-based control law

Once the desired trajectory of the mothership is calculated using methods from the previous section, a Lyapunov-based backstepping approach (Khalil, 2002) can be used to find the control inputs that cause the mothership to track that trajectory. This is inspired, in part, by the work of Skjetne et al. (2004) and Aguiar and Hespanha (2007). Skjetne et al. (2004) proposes an output maneuvering controller for a class of strict feedback nonlinear processes and applies it to path-following for fully actuated ships. Aguiar and Hespanha (2007) combine adaptive switching supervisory control with a nonlinear Lyapunov-based (backstepping) tracking control law for underactuated autonomous vehicles.

The dynamic equations of the mothership can be written as

$$
\begin{aligned}
\dot{p_n} &= V\cos\chi\cos\gamma \\
\dot{p_e} &= V\sin\chi\cos\gamma \\
\dot{p_d} &= -V\sin\gamma \\
\dot{V} &= -g\sin\gamma - \frac{D}{m} + \frac{1}{m}T + \frac{F_v}{m} \\
\dot{\gamma} &= -\frac{g}{V}\cos\gamma\cos\phi + \frac{g}{V}(\cos\phi)n + \frac{F_\chi}{mV\cos\gamma} \\
\dot{\chi} &= \frac{L}{mV\cos\gamma}\sin\phi + \frac{F_\gamma}{mV} \\
\dot{\phi} &= u_\phi
\end{aligned}
$$

where $n = \frac{L}{mg}$ is the (controlled) load factor. The control inputs are the thrust T, load factor n, and roll angle command u_ϕ. The tension forces in the inertial coordinate system can be expressed in velocity coordinates via the transformation

$$
\begin{pmatrix} F_V \\ F_\chi \\ F_\gamma \end{pmatrix} = \begin{pmatrix} \cos\gamma\cos\chi & \cos\gamma\sin\chi & \sin\gamma \\ -\sin\chi & \cos\chi & 0 \\ -\sin\gamma\cos\chi & -\sin\gamma\sin\chi\cos\gamma \end{pmatrix} \begin{pmatrix} T^x_1 \\ T^y_1 \\ T^z_1 \end{pmatrix},
$$

where (T^x_1, T^y_1, T^z_1) are the components of tension in the inertial frame for the first cable element connected to the mothership.

Assuming that the desired trajectory $\mathbf{p^d}(t) \in \mathbf{R}^3$ is smooth (it has derivatives of all orders), and defining the candidate inputs as $\mathbf{u_c} \triangleq (T, n, \sin\phi)^T$, then rearranging the dynamic equations of the mothership yields

$$
\begin{pmatrix} \dot{V} \\ \dot{\gamma} \\ \dot{\chi} \end{pmatrix} = \begin{pmatrix} -g\sin\gamma - \frac{D}{m} + \frac{F_v}{m} \\ -\frac{g}{V}\cos\gamma\cos\phi + \frac{F_\chi}{mV\cos\gamma} \\ \frac{F_\gamma}{mV} \end{pmatrix} + \begin{pmatrix} \frac{1}{m} & 0 & 0 \\ 0 & \frac{g}{V}\cos\phi & 0 \\ 0 & 0 & \frac{L}{mV\cos\gamma} \end{pmatrix} \begin{pmatrix} T \\ n \\ \sin\phi \end{pmatrix}
$$

$$= \mathbf{F} + \mathbf{G}\mathbf{u_c},$$

where

$$\mathbf{F} = \begin{pmatrix} -g\sin\gamma - \frac{D}{m} + \frac{F_v}{m} \\ -\frac{g}{V}\cos\gamma\cos\phi + \frac{F_\chi}{mV\cos\gamma} \\ \frac{F_\gamma}{mV} \end{pmatrix}, \ \mathbf{G} = \begin{pmatrix} \frac{1}{m} & 0 & 0 \\ 0 & \frac{g}{V}\cos\phi & 0 \\ 0 & 0 & \frac{L}{mV\cos\gamma} \end{pmatrix}, \ \mathbf{u_c} = \begin{pmatrix} T \\ n \\ \sin\phi \end{pmatrix}.$$

Step 1. Error dynamics: Let $\mathbf{e} \triangleq \mathbf{p} - \mathbf{p^d}$ be the tracking error in the inertial frame, where $\mathbf{p} = (p_n, p_e, p_d)^T$ is the location of the mothership. The dynamic equation for the inertial tracking error is then given by

$$\dot{\mathbf{e}} = \dot{\mathbf{p}} - \dot{\mathbf{p}}^{\mathbf{d}}.$$

Step 2. Error convergence: Define the Lyapunov candidate function $V_1 \triangleq \frac{1}{2}\mathbf{e}^T\mathbf{e}$, which has the time derivative

$$\begin{aligned} \dot{V}_1 &= \mathbf{e}^T\dot{\mathbf{e}} \\ &= \mathbf{e}^T(\dot{\mathbf{p}} - \dot{\mathbf{p}}^{\mathbf{d}}). \end{aligned} \tag{9}$$

At this stage of the development, we consider $\dot{\mathbf{p}}$ as a virtual control, where $\dot{V}_1$ can be made negative definite by setting $\dot{\mathbf{p}}$ equal to $\dot{\mathbf{p}}^{\mathbf{d}} - k_1\mathbf{e}$ for some positive constant k_1. Introducing the error variable

$$\mathbf{z^d} \triangleq \dot{\mathbf{p}}^{\mathbf{d}} - k_1\mathbf{e},$$

and adding and subtracting $-k_1\mathbf{e}^T\mathbf{e}$ in Equation (9) gives

$$\dot{V}_1 = -k_1\mathbf{e}^T\mathbf{e} + \mathbf{e}^T(\dot{\mathbf{p}} - \mathbf{z^d}).$$

Step 3. Backstepping for $\mathbf{z^d}$*:* Consider the augmented Lyapunov candidate function

$$V_2 \triangleq V_1 + \frac{1}{2}(\dot{\mathbf{p}} - \mathbf{z^d})^T(\dot{\mathbf{p}} - \mathbf{z^d}) = \frac{1}{2}\mathbf{e}^T\mathbf{e} + \frac{1}{2}(\dot{\mathbf{p}} - \mathbf{z^d})^T(\dot{\mathbf{p}} - \mathbf{z^d}),$$

with Lie derivative

$$\dot{V}_2 = -k_1\mathbf{e}^T\mathbf{e} + (\dot{\mathbf{p}} - \mathbf{z^d})^T(\mathbf{e} + \ddot{\mathbf{p}} - \dot{\mathbf{z}}^{\mathbf{d}}).$$

From the mothership dynamic equations, we have

$$\begin{aligned} \ddot{\mathbf{p}} &= \begin{pmatrix} \cos\gamma\cos\chi & -V\sin\gamma\cos\chi & -V\cos\gamma\sin\chi \\ \cos\gamma\sin\chi & -V\sin\gamma\sin\chi & -V\cos\gamma\cos\chi \\ -\sin\gamma & -V\cos\gamma & 0 \end{pmatrix} \begin{pmatrix} \dot{V} \\ \dot{\gamma} \\ \dot{\chi} \end{pmatrix} \\ &= \mathbf{M}(\mathbf{F} + \mathbf{G}\mathbf{u_c}), \end{aligned}$$

where

$$\mathbf{M} \triangleq \begin{pmatrix} \cos\gamma\cos\chi & -V\sin\gamma\cos\chi & -V\cos\gamma\sin\chi \\ \cos\gamma\sin\chi & -V\sin\gamma\sin\chi & -V\cos\gamma\cos\chi \\ -\sin\gamma & -V\cos\gamma & 0 \end{pmatrix}.$$

Therefore

$$\dot{V}_2 = -k_1\mathbf{e}^T\mathbf{e} + (\dot{\mathbf{p}} - \mathbf{z^d})^T(\mathbf{e} + \mathbf{MF} + \mathbf{MGu_c} - \dot{\mathbf{z}}^\mathbf{d}).$$

By constraining V, γ, and χ to reasonable values, the matrices $\mathbf{M}$ and $\mathbf{G}$ will be full rank. The product of two full-rank matrices is also full rank, and therefore $\mathbf{MG}$ is invertible. Define

$$\xi \triangleq (\mathbf{MG})^{-1}[\dot{\mathbf{z}}^\mathbf{d} - \mathbf{MF} - \mathbf{e} - k_2(\dot{\mathbf{p}} - \mathbf{z^d})],$$

where k_2 is a positive constant, and

$$\eta \triangleq \sin\phi.$$

If we select

$$\begin{pmatrix} T \\ n \end{pmatrix} = \begin{pmatrix} 1\,0\,0 \\ 0\,1\,0 \end{pmatrix}\xi, \tag{10}$$

and

$$z_2^d \triangleq \eta - \begin{pmatrix} 0\,0\,1 \end{pmatrix}\xi,$$

then the time derivative of the z_2^d can be written as

$$\begin{aligned} \dot{z_2}^d &= \dot{\eta} - \begin{pmatrix} 0\,0\,1 \end{pmatrix}\dot{\xi} \\ &= u_\phi\cos\phi - \begin{pmatrix} 0\,0\,1 \end{pmatrix}\dot{\xi}, \end{aligned}$$

and

$$\mathbf{u_c} = \begin{pmatrix} T \\ n \\ \eta \end{pmatrix} = \xi + z_2^d \begin{pmatrix} 0 \\ 0 \\ 1 \end{pmatrix}.$$

Thus

$$\dot{V}_2 = -k_1\mathbf{e}^T\mathbf{e} - k_2(\dot{\mathbf{p}} - \mathbf{z^d})^T(\dot{\mathbf{p}} - \mathbf{z^d}) + (\dot{\mathbf{p}} - \mathbf{z^d})^T(\mathbf{MG}\begin{pmatrix} 0 \\ 0 \\ 1 \end{pmatrix} z_2^d).$$

Step 4. Backstepping for z_2^d: Consider the augmented Lyapunov candidate function

$$V_3 \triangleq V_2 + \frac{1}{2}(z_2^d)^2,$$

with the time derivative

$$\dot{V}_3 = -k_1\mathbf{e}^T\mathbf{e} - k_2(\dot{\mathbf{p}} - \mathbf{z^d})^T(\dot{\mathbf{p}} - \mathbf{z^d}) + z_2^d(\dot{z}_2^d + (\dot{\mathbf{p}} - \mathbf{z^d})^T\mathbf{MG}\begin{pmatrix}0\\0\\1\end{pmatrix})$$

$$= -k_1\mathbf{e}^T\mathbf{e} - k_2(\dot{\mathbf{p}} - \mathbf{z^d})^T(\dot{\mathbf{p}} - \mathbf{z^d}) + z_2^d(u_\phi\cos\phi - \begin{pmatrix}0&0&1\end{pmatrix}\dot{\xi} + (\dot{\mathbf{p}} - \mathbf{z^d})^T\mathbf{MG}\begin{pmatrix}0\\0\\1\end{pmatrix}).$$

If we choose

$$u_\phi = \frac{1}{\cos\phi}[\begin{pmatrix}0&0&1\end{pmatrix}\dot{\xi} - (\dot{\mathbf{p}} - \mathbf{z^d})^T\mathbf{MG}\begin{pmatrix}0\\0\\1\end{pmatrix} - k_3 z_2^d], \tag{11}$$

where k_3 is a positive constant, then the time derivative of V_3 becomes

$$\dot{V}_3 = -k_1\mathbf{e}^T\mathbf{e} - k_2(\dot{\mathbf{p}} - \mathbf{z^d})^T(\dot{\mathbf{p}} - \mathbf{z^d}) - k_3(z_2^d)^2 \leq 0. \tag{12}$$

Therefore, according to the Lyapunov stability theorem (Khalil, 2002), the point $(\mathbf{e}^T, (\dot{\mathbf{p}} - \mathbf{z^d})^T, z_2^d)^T = \mathbf{0}$ is uniformly asymptotically stable, and from Equation(12) we have

$$V_3(t) \leq V_3(0)$$
$$\|\mathbf{e}(t)\|^2 + \left\|\dot{\mathbf{p}}(t) - \mathbf{z^d}(t)\right\|^2 + [(z_2^d(t)]^2 \leq \|\mathbf{e}(0)\|^2 + \left\|\dot{\mathbf{p}}(0) - \mathbf{z^d}(0)\right\|^2 + [(z_2^d(0)]^2.$$

Thus by the appropriate selection of k_1, k_2, and k_3, $\mathbf{e}$ is bounded and converges to a neighborhood of the origin. The control inputs (T, n, u_ϕ) are given by Equation (10) and (11).

3.3 Mothership path planning and control simulation results

In this section, the methods developed in Sections 3.1 and 3.2 are used to simulate trajectory calculation and control of the mothership, given a desired drogue orbit. Table 2 contains the parameters used in the simulation. The desired circular trajectory $(p_n^{dr}, p_e^{dr}, p_d^{dr})$ of the drogue can be written in parametric form as

$$p_n^{dr}(t) = R^{dr}\sin(\frac{V^{dr}}{R^{dr}}t)$$
$$p_e^{dr}(t) = R^{dr}\cos(\frac{V^{dr}}{R^{dr}}t)$$
$$p_d^{dr}(t) = -900 \text{ m},$$
$$t = [0, +\infty).$$

where R^{dr} and V^{dr} are defined in Table 2. The desired initial position $(p_n^m(0), p_e^m(0), p_d^m(0))$, velocity V^m, and radius R^m of mothership to achieve the specified drogue orbit may be calculated using the differential flatness property:

$$\begin{aligned}(p_n^m(0), p_e^m(0), p_d^m(0)) &= (99.57,\ 96.86,\ -908.71)\ \text{m}\\ V^m &= 20.84\ \text{m/s}\\ R^m &= 138.91\ \text{m}.\end{aligned}$$

Thus the initial position error of the mothership is $(-99.57,\ 33.14,\ 91.29)$ m. Figure 6 shows simulation results of the desired and actual trajectories of the mothership, as well as the tracking error in the absence of wind. We see that the mothership tracks the desired trajectory after a 50 second transient. Figure 7 shows simulation results of the desired and actual trajectories of the drogue, as well as the tracking error in the absence of wind. We see that the drogue converges to its desired trajectory after a 70 second transient. Figure 8 shows the time evolution of the characteristic parameters of the mothership. Since the initial position error of the mothership is large compared to the airspeed of the mothership, the control inputs all go to their limits in the first 50 second transient, and after that the mothership enters a steady state. The tension force in the cable acts on the mothership in the centripetal direction. The result is that, even though the roll angle ϕ goes to zero in the steady state, the mothership is still able to fly in a circular orbit.

Table 2 Parameters for simulation of mothership orbit calculation and control

Mothership	Initial Position	Velocity Range	Mass
	(0, 130, -1000) m	18-27 m/s	1.76 kg
Drogue	Desired Airspeed	Desired Altitude	Desired Orbit Radius
	$V^{dr} = 15$ m/s	900 m	$R^{dr} = 100$ m
Cable	Mass	Length	Diameter
	0.01 kg	100 m	0.01 m
MAV	Airspeed		
	16.67 m/s		

4 Active drogue control for improved orbit tracking

The previous section described a method for controlling the orbit of a passive drogue indirectly through path planning and control of the mothership. In this section we present a method to control the drogue orbit directly through drag modulation, with the objective of improving upon the control achieved through indirect control alone. It is assumed that the drogue is fitted with drag-inducing spoilers.

Most towed-cable systems described in the literature (e.g., Skop and Choo, 1971; Murray, 1996; Turkyilmaz and Egeland, 2001; Williams and Trivailo, 2007a,b,a; Williams et al., 2008) are based on a passive (unactuated) drogue. Our

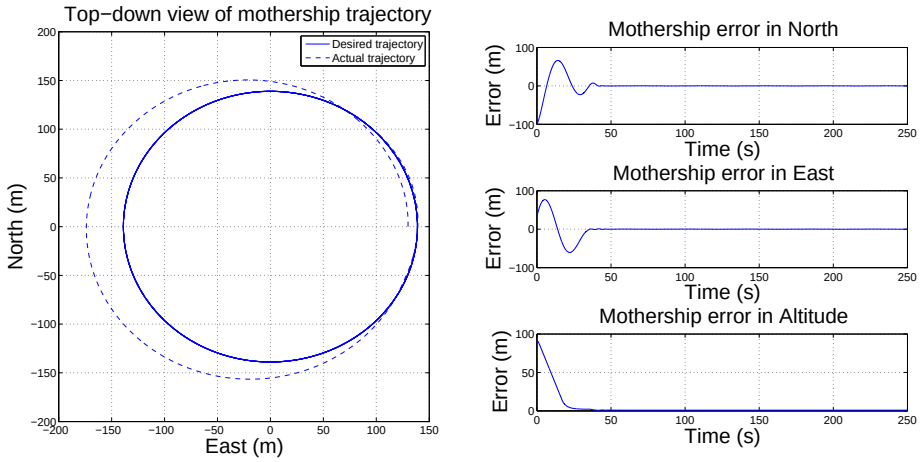

Figure 6 Mothership trajectory and error driven by Lyapunov-based backstepping control law in the absence of wind.

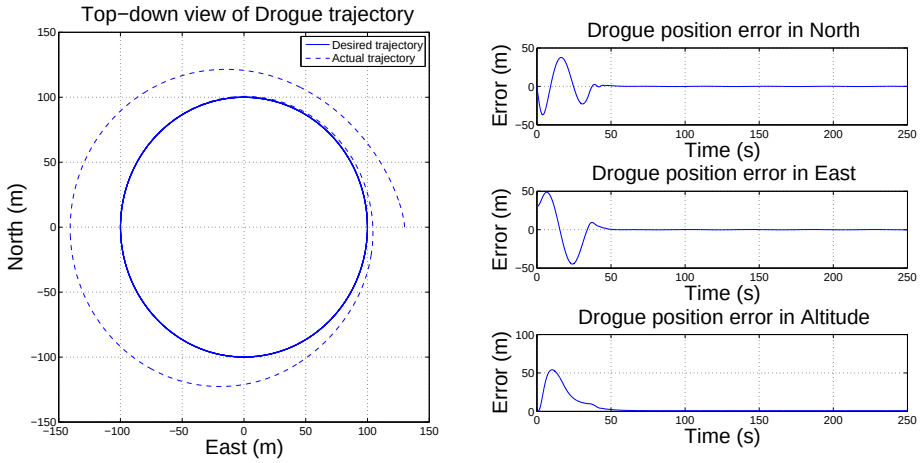

Figure 7 Drogue trajectory and error driven by Lyapunov-based backstepping control law in the absence of wind

approach is motivated by Skop and Choo (1971), which shows that under zero-wind conditions, if the mothership flies in a constant-angular-rate orbit of radius R, and the drogue has sufficient aerodynamic drag, then the motion of the drogue has a stable orbit of radius $r \ll R$. Since the angular rates of the towplane and the drogue are identical, i.e.,

$$\omega = \frac{V_m}{R} = \frac{V_N}{r},$$

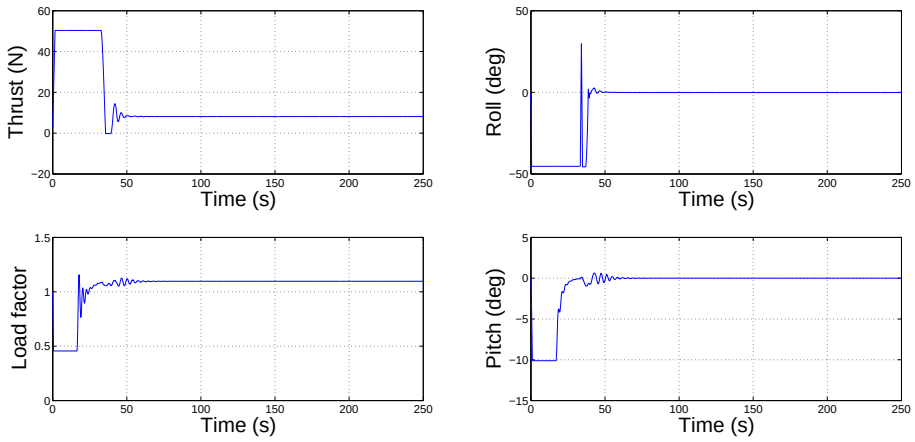

Figure 8 Time evolution of the thrust T, load factor n, roll angle ϕ, path angle γ of the mothership.

where ω is the angular rate of the towplane and the drogue, and the V_m and V_N are the airspeeds of the mothership and the drogue, respectively, then

$$V_N = r\frac{V_m}{R}. \tag{13}$$

Therefore, we can regulate the drogue to a desired radius r^d by regulating the velocity of the drogue to $V_N^d = r^d V_m/R$. A simple method to regulate drogue velocity is to add spoilers to the drogue and to regulate the spoilers with the control law

$$C_{D_N} = (K_P + \frac{K_I}{s})(V_N - V_N^d),$$

where C_{D_N} is the (spoiler-controlled) drag coefficient, V_N^d is the desired airspeed of the drogue, V_N is the current airspeed, s is the Laplace variable, and K_P and K_I are positive proportional and integral gains, respectively.

4.1 Active drogue control simulation results

Simulations were created to demonstrate that the drag coefficient can be used effectively to control the drogue radius. To compare the difference between the drogue motion with and without active control, the drag controller is switched on at $t = 150$ s. Given the parameters in Table 1, if the desired drogue radius is 60 m, then the desired drogue velocity is $V_N^d = 10$ m/s (see (Equation 13)). Figure 9 shows that the steady state radius of the drogue converges to a smaller radius that oscillates between 54 m and 58 m. The steady state drogue velocity oscillates between 9 and 9.5 m/s, allowing the chasing MAV to overtake and rendezvous with the drogue.

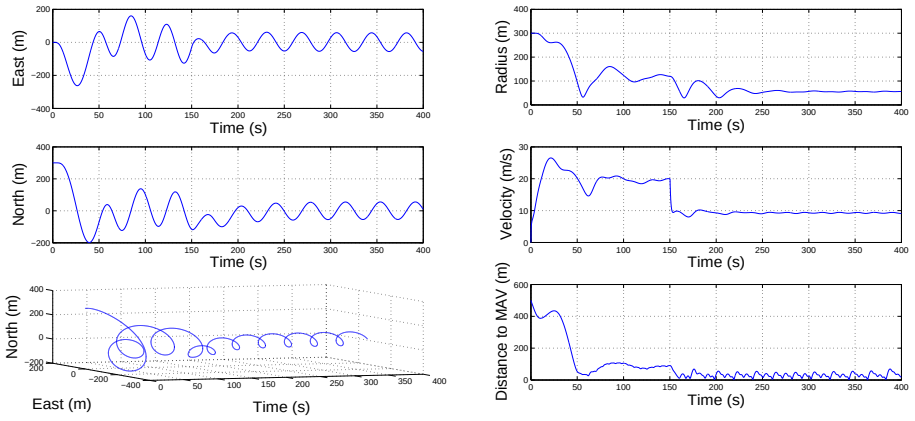

Figure 9 Simulation of drogue motion using active drag control. Shows north and east motion of the drogue (left) and the radius, velocity and distance to the MAV of the drogue (right). Drag control is activated at $t = 150$ s. The steady state radius is smaller than without drag control.

5 MAV orbit estimation

In previous sections, a method was described for achieving a desired drogue orbit by controlling the orbit of the mothership and the drag of the drogue. The purpose of this section is to describe methods for another important element of MAV-drogue rendezvous: the mathematical description of the drogue's orbit and the estimation of the orbit parameters from GPS data. In Section (6) we discuss methods to enable the MAV to track the drogue orbit in preparation for final rendezvous. For this paper, it is assumed that there is communication between the drogue and MAV, allowing the drogue to transmit its position and heading (from an on-board GPS receiver) to the MAV. The drogue orbit is estimated from the transmitted data and a coordinated rendezvous approach is taken, rather than treating the drogue as a target during the initial stages of rendezvous. The MAV assumes the same orbit as the drogue, allowing a more natural initial rendezvous approach. During the final stages of rendezvous, when the relative position between the MAV and drogue is small, it is necessary to use some other rendezvous algorithm (e.g., vision-based proportional navigation). This section focuses on the problem of estimating the drogue orbit from GPS data. Section 6 describes a method that enables the MAV to track the drogue orbit. Future work will address the final approach and docking of the MAV and drogue through the use of vision-aided proportional navigation, such as that described in (Barber et al., 2007). This work is, in some ways, related to research on autonomous aerial refueling of UAVs, which has been proposed using vision alone (Kimmett et al., 2002) and integrated vision and GPS (Mammarella et al., 2008). Unlike work on aerial refueling, however, aerial recovery research must address the issue of dissimilar speeds of the mothership and MAV. Furthermore, in the approach taken in this paper the MAV must travel in a

circular or elliptical path to achieve docking with the drogue, whereas docking for aerial refueling can be accomplished with roughly linear trajectories.

Ideally, the drogue will travel in a circular orbit in a plane parallel to the ground. In practice, the actual drogue orbit is not circular and in the horizontal plane due to (1) wind and other disturbances, and (2) the numerical approximations inherent in the inverse dynamics to find the required mothership orbit from the desired circular drogue orbit. Consequently, for estimation purposes, the drogue orbit will be treated as an arbitrarily rotated ellipse. The parametric equations for a planar elliptical orbit are given by

$$\begin{aligned} x - x_0 &= a\cos(t)\cos(\psi) - b\sin(t)\sin(\psi) \\ y - y_0 &= a\cos(t)\sin(\psi) + b\sin(t)\cos(\psi) \end{aligned} \tag{14}$$

where x_0 and y_0 describe the center of the ellipse, a and b are the major and minor axes respectively, and ψ is the angle of rotation of the ellipse measured from the x-axis. The strategy taken in this paper is to estimate the orbit along which the drogue is traveling, projected onto the plane parallel to the ground. The MAV tracks that orbit using a longitudinal controller, and a separate control loop is used to match the MAV and drogue altitudes.

5.1 Fitzgibbon's method

Early numerical methods for estimating the parameters of an ellipse were based on general conic fitting, which could result in estimates that actually represented other conics (hyperbolas or parabolas). Fitzgibbon et al. (1999) developed a constrained least-squares fitting method for ellipses by including a constraint to guarantee that the solution must be an ellipse. Fitzgibbon's approach begins with the general equation for a conic,

$$F(x, y) = a_1x^2 + a_2xy + a_3y^2 + a_4x + a_5y + a_6 = 0, \tag{15}$$

and adds an ellipse-specific constraint given by

$$4a_1a_3 - a_2^2 > 0. \tag{16}$$

This is an inequality constraint, requiring that the left side of the equation be greater than zero to result in the equation of an ellipse. It has been shown that recasting this as an equality constraint, in which (16) is still satisfied, results in valid parameter estimates whose values are not dependent on the particular constant value used on the right side of (16). Essentially, since (15) can be multiplied by a constant and the result is the same ellipse, (16) can be set to an arbitrary constant without loss of generality. Thus (16) can be written as

$$4a_1a_3 - a_2^2 = 1, \tag{17}$$

where the right side of the equality is arbitrarily set to the value of 1. This procedure is desirable because the solution of the constrained optimization problem is more straightforward for the case of equality constraints. Using the method of

Lagrange multipliers proposed by Gander (1981), the estimation problem can be posed as

$$\mathbf{D^T D a} = \lambda \mathbf{C a} \text{ subject to } \mathbf{a^T C a} = 1, \tag{18}$$

where

$$\mathbf{D} = \begin{pmatrix} x_1^2 & x_1 y_1 & y_1^2 & x_1 & y_1 & 1 \\ \vdots & \vdots & \vdots & \vdots & \vdots & \vdots \\ x_i^2 & x_i y_i & y_i^2 & x_i & y_i & 1 \\ \vdots & \vdots & \vdots & \vdots & \vdots & \vdots \\ x_N^2 & x_N y_N & y_N^2 & x_N & y_N & 1 \end{pmatrix}, \tag{19}$$

$$\mathbf{C} = \begin{pmatrix} 0 & 0 & 2 & 0 & 0 & 0 \\ 0 & -1 & 0 & 0 & 0 & 0 \\ 2 & 0 & 0 & 0 & 0 & 0 \\ 0 & 0 & 0 & 0 & 0 & 0 \\ 0 & 0 & 0 & 0 & 0 & 0 \end{pmatrix}, \tag{20}$$

and

$$\mathbf{a} = \begin{bmatrix} a_1 & a_2 & a_3 & a_4 & a_5 & a_6 \end{bmatrix}^T. \tag{21}$$

Solving (18) yields six possible solutions for $\mathbf{a}$; the correct least-squares solution is the eigenvector that corresponds to the smallest positive eigenvalue. These general ellipse parameters can be used to solve for the parameters in the parametric equations of an ellipse, described by (14).

5.2 Numerically stable improvement

Fitzgibbon's method has the drawback that the computation of the eigenvalues is sometimes unstable and can yield infinite or complex results. This arises from the fact that $\mathbf{D}^T\mathbf{D}$ is often nearly singular. Halir and Flusser (1998) proposed a method for improving the accuracy and speed of the algorithm. This method, which is based on Fitzgibbon's method, makes use of the special structure of the matrices to eliminate the singularities. The result is unstable only if all of the points lie on the same line, in which case there is no suitable approximation for an ellipse.

5.3 Recursive least squares

The method introduced by Halir and Flusser is used to obtain an estimate of orbit parameters from the first several GPS data points provided by the drogue. Once an initial estimate of the orbit is calculated using this method, recursive least squares (RLS) (Moon and Sterling, 2000) is used to update the estimate for each new GPS data point received from the drogue. The parameters to estimate are again represented by the vector $\mathbf{a}$ defined in Equation (21). The parameter estimates are updated using the following equations:

$$\gamma_{n+1} = \frac{1}{\lambda + \mathbf{x}_{n+1}^T \mathbf{P}_n \mathbf{x}_{n+1}}$$
$$\mathbf{a}_{n+1} = \mathbf{a}_n - \gamma_{n+1} \mathbf{P}_n \mathbf{x}_{n+1} \mathbf{x}_{n+1}^T \mathbf{a}_n$$
$$\mathbf{P}_{n+1} = \frac{1}{\lambda} \left(\mathbf{P}_n - \gamma_{n+1} \mathbf{P}_n \mathbf{x}_{n+1} \mathbf{x}_{n+1}^T \mathbf{P}_n \right),$$

where $\mathbf{P}$ is initialized as the identity matrix. The vector $\mathbf{x}$ represents the most recent GPS data received from the drogue, and λ is the forgetting factor, which controls the responsiveness of the estimates and the level of filtering.

5.4 MAV orbit estimation simulation results

The Halir-Flusser method followed by RLS was applied to simulated GPS data from the drogue, with additive Gaussian noise with a standard deviation of 5 m. Figure 10 shows the resulting estimated elliptical orbit. Figure 11 shows the evolution of the estimate of x_0 (the north position of the center of the ellipse) as new GPS data points are included in the recursion. It is clear that the estimate converges to the true value of 50 m. Figure 12 shows the evolution of the estimate of the ellipse major axis. Again, the estimate converges to the true value. Estimates for the other ellipse parameters (minor axis, rotation angle, and east location of the center) follow similar trends.

6 MAV orbit tracking

The objective is for the MAV to insert itself onto the drogue orbit at a point behind the drogue, and then track the orbit at a speed slightly greater than that of the drogue until rendezvous occurs. This section describes methods that enable the MAV to enter and track the drogue orbit. The approach taken in this paper is to decouple longitudinal control (for altitude tracking) from lateral control (for horizontal orbit tracking). The horizontal orbit is the elliptical projection of the drogue orbit onto the horizontal plane, which is estimated using the methods described in the previous section.

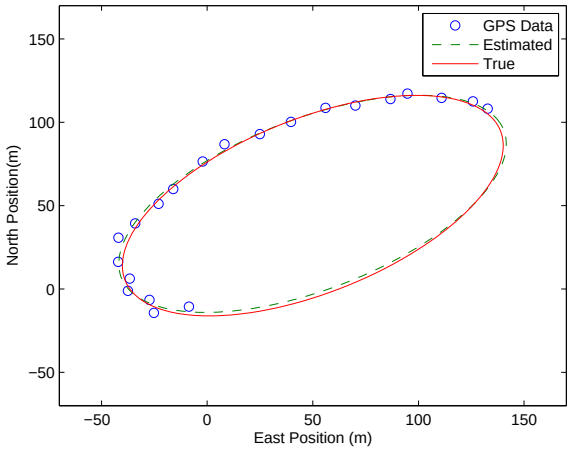

Figure 10 Estimated orbit from simulated noisy data.. The solid line represents the true orbit. The circles represent simulated noisy GPS data points. The dashed line represents the estimated orbit.

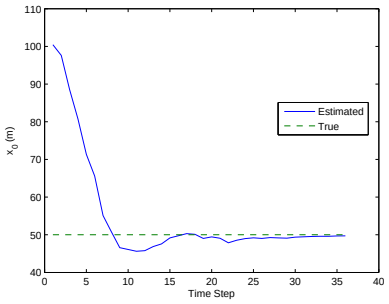

Figure 11 Estimate of x_0 using the Halir-Flusser method and RLS

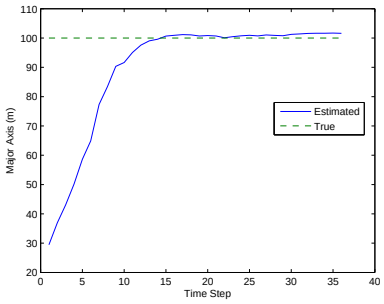

Figure 12 Estimate of the ellipse major axis using the Halir-Flusser method and RLS

6.1 Lateral control

The lateral control to achieve elliptical orbit tracking of the MAV is done using a vector field method Nelson et al. (2007). Whether the MAV is on or off of the elliptical orbit, its desired heading is calculated using

$$\begin{aligned} dy &= -b^2\left(x - x_0\right) + \frac{k(y-y_0)}{a}\left(1 - \frac{(x-x_0)^2}{a^2} - \frac{(y-y_0)^2}{b^2}\right) \\ dx &= a^2\left(y - y_0\right) + \frac{k(x-x_0)}{a}\left(1 - \frac{(x-x_0)^2}{a^2} - \frac{(y-y_0)^2}{b^2}\right) \end{aligned} \tag{22}$$

and

$$\tan(\psi) = \frac{\partial y}{\partial x}. \tag{23}$$

Figure 13 shows a simulation of the MAV entering and tracking an elliptical orbit using the vector field approach. In this simulation, the MAV starts in the center of the ellipse, enters the elliptical orbit, and executes a complete orbit. The MAV tracks the orbit to within one meter, as shown in Figure 14.

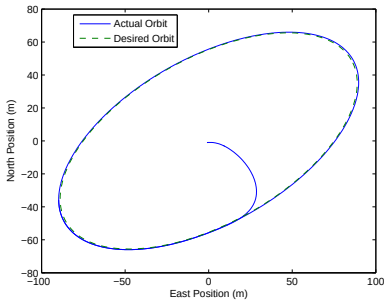

Figure 13 Elliptical orbit tracking. The dashed line represents the drogue orbit, and the solid line represents the MAV trajectory as it tracks the desired orbit, starting from an initial position at the center of the orbit.

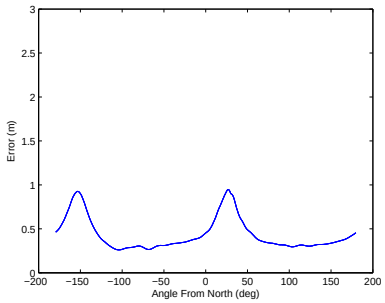

Figure 14 Error in tracking an elliptical orbit for a single orbit. The error is consistently less than 1 m for all locations on the orbit.

6.2 Longitudinal control

The longitudinal control of the MAV is used to match the altitude of the MAV to that of the drogue. The commanded altitude for the MAV is the altitude of the drogue at its current position. The autopilot calculates a desired angle of attack for the MAV using a PID controller. In simulation, the altitude of the MAV matches the altitude of the drogue to within 1 m for an entire orbit..

7 Flight test results

Flight tests were conducted to demonstrate the mothership-drogue interactions modeled in previous sections. In these tests, the mothership (a twin prop, 55-inch wingspan, battery-powered, autonomous aircraft with a Kestrel autopilot; see Figure 15) was hand launched while towing a hemispherical drogue instrumented with a GPS data logger (Figure 16).

The mothership autonomously maintained a specified circular orbit, and the resulting orbit of the drogue was observed using the on-board GPS data logger. Figure 17 shows the mothership and drogue orbits in the horizontal plane. In this

case the specified radius of the mothership was approximately 85 m, the mothership velocity was 14 m/s, and the cable length was 125 m. The resulting orbit radius and velocity of the drogue were 55 m and 9 m/s, respectively. This result illustrates the feasibility of achieving stable drogue orbits at a smaller radius and decreased speed, which is a necessity for aerial MAV recovery, and confirms the simulation results presented in Section 2. Figure 18 shows the orbits of the mothership and drogue in the North-vertical plane. Due to wind, the drogue orbit is tilted out of the horizontal plane, despite the horizontal mothership orbit. This validates the approach taken in Section 5, in which the drogue orbit was treated as an out-of-plane ellipse, and parameters of the projection of this ellipse on the horizontal plane were estimated. Furthermore, the advantages of utilizing decoupled altitude and orbit tracking control laws, as described in Section 6, are also reinforced. Although a MAV did not track the drogue orbit in this set of experiments, the results show a relatively consistent and stable drogue orbit that could be estimated and tracked by a MAV in future experiments.

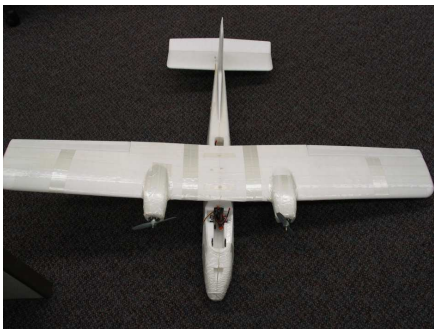

Figure 15 Mothership used in preliminary flight tests

Figure 16 Hemispherical drogue used in preliminary flight tests

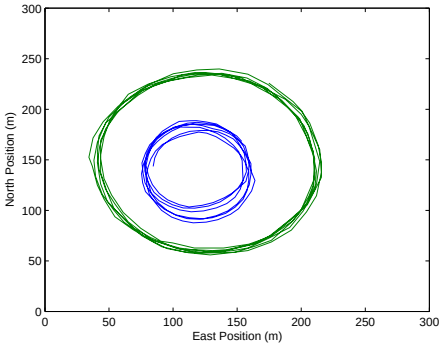

Figure 17 Experimental orbits of mothership and drogue with 125 m cable and mothership velocity of 13.5 m/s

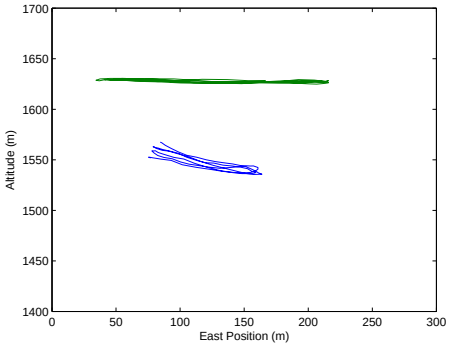

Figure 18 Experimental altitude data for mothership and drogue with 125 m cable and mothership velocity of 13.5 m/s

8 Conclusions and future work

In this paper we presented a novel approach to the aerial recovery problem for micro air vehicles. In this approach, a mothership tows a drogue that establishes a stable orbit at a speed that is slow enough to allow the MAV to overtake the drogue as it moves along its orbit trajectory. The approach is motivated by the need to have a small relative velocity between the MAV and the recovery vehicle, which is not practical if the mothership is to capture the MAV directly. The focus of this work is on modeling the system's dynamics, developing mothership control laws to enforce drogue orbits, developing methods to enable a MAV to estimate elliptical drogue orbits, and designing control laws to allow the MAV to track the drogue. A novel multi-link dynamic model, based on Gauss's Principle, has been shown to accurately represent the mothership-cable-drogue dynamics, and a simulation environment was developed to enable simulation of mothership-drogue dynamic interactions. An inverse dynamics method for calculating the required mothership orbit to achieve a desired drogue orbit was also presented. Using a Lyapunov-based backstepping approach, a control law was designed to enable stable tracking of the required orbit by the mothership. Experimental results demonstrated the feasibility of controlling the mothership to establish a stable orbit of a towed drogue. An approach to controlling the drogue directly, using drag coefficient control, was developed and simulated, showing that it is feasible to control the drogue orbit by changing the drag of the drogue. Finally, methods to enable the MAV to estimate and track the drogue orbit were developed. These methods will allow the MAV to synchronize its motion with that of the drogue, in preparation for a final coordinated rendezvous.

The methods developed in this work are essential components of aerial recovery of MAVs. Their feasibility was demonstrated through simulation and experimental flight test results. Although we have addressed some of the key questions in aerial recovery, many important challenges remain that will be addressed in future work. First, the trajectory generation method should be able to account for wind, allowing the mothership to modify its orbit to result in an essentially flat drogue orbit in the presence of wind. In the flight tests presented in this paper, we showed that wind disturbances result in non-horizontal drogue orbits. Current work seeks to address this problem by (1) designing appropriate inclined mothership orbits to result in horizontal drogue orbits in the presence of wind, and (2) employing active drogue control (via spoilers and active tether extension/contraction control) to compensate for wind disturbances. Future work will advance these approaches through control design, simulations, and additional flight tests. Second, improvements must be made to the recursive orbit estimation algorithms presented in this paper to guarantee that the recursive estimates describe an ellipse, and not some other conic. A Kalman filter with nonlinear state constraints is being explored as a solution to this problem (Julier and LaViola, 2007; Yang and Blasck, 2006; Simon and Chia, 2002). Third, methods must be developed to allow the MAV, which is traveling behind the drogue in a stable orbit, to approach and dock with the drogue. We are exploring the use of vision-aided proportional navigation, such as that described in (Barber et al., 2007), in which a MAV tracks and lands in the back of a moving truck. Ongoing experimental flight tests will allow us to validate and refine each component of the aerial recovery process.

Acknowledgments

This work was funded by AFOSR contract FA9550-09-C-0102.

References

Aguiar, A. P. and Hespanha, J. P. 2007. Trajectory-tracking and path-following of underactuated autonomous vehicles with parametric modeling uncertainty. *IEEE Transactions on Automatic Control*, 52(8):1362–1379.

Barber, D. B., Griffiths, S. R., McLain, T. W., and Beard, R. W. 2007. Autonomous landing of miniature aerial vehicles. *AIAA Journal of Aerospace Computing, Information, and Communication*, 4:70–84.

Chin, C.K.H., a. M. R. and Connell, H. 2000. A numerical model of a towed cable-body system. *ANZIAM Journal*, 42:C362–C384.

Choo, Y. and Casarella, M. J. 1973. A survey of analytical methods for dynamic simulation of cable-body systems. *Journal of Hydronautics*, 7(4):137–144.

Cochran, J., Innocenti, M., No, T., and Thukral, A. 1992. Dynamics and control of maneuverable towed flight vehicles. *JGCD*, 15(5):1245–1252.

Fitzgibbon, A., Pilu, M., and Fisher, R. B. 1999. Direct least square fitting of ellipses. *IEEE Transactions on Pattern Analysis and Machine Intelligence*, 21:476–480.

Fliess, M., Levine, J., Martin, P., and Rouchon, P. 1995. Flatness and defect of nonlinear systems: Theory and examples. *Int. J. Control*, 61(6):1327–1361.

Gander, W. 1981. Least squares with a quadratic constraint. *Numerische Mathematik*, 36:291–307.

Halir, R. and Flusser, J. 1998. Numerically stable least squares fitting of ellipses. In *Proceedings of the 6th International Conference in Central Europe on Computer Graphics and Visualization*.

Julier, S. J. and LaViola, J. J. 2007. On kalman filtering with nonlinear equality constraints. *IEEE Transactions on Signal Processing*, 55(6):2774–2784.

Khalil, H. K. 2002. *Nonlinear Systems*. Prentice Hall.

Kimmett, J., Valasek, J., and Junkins, J. L. 2002. Vision based controller for autonomous aerial refueling. In *Proceedings of the 2002 IEEE International Conference on Control Applications*.

Lu, W. C., Duan, L., Fei-Bin, H., and Mora-Camino, F. 2008. Differential flatness applied to vehicle trajectory tracking. In *Proc. 27th Chinese Control Conference CCC 2008*, pages 242–247.

Lu, W. C., Faye, R. M., Ramos, A. C. B., Slama, J., and Mora-Camino, F. 2007. Neural inversion of flight guidance dynamics. In *Proc. Seventh International Conference on Intelligent Systems Design and Applications ISDA 2007*, pages 190–195.

Lu, W. C., Mora-Camino, F., and Achaibou, K. 2005. A flatness based flight guidance control using neural networks. In *Proc. 24th Digital Avionics Systems Conference DASC 2005*, volume 1, pages 6.C.1–6.1–7.

Mammarella, M., Campa, G., Mapolitano, M. R., Fravolini, M. L., Gu, Y., and Perhinschi, M. G. 2008. Machine vision/gps integration using ekf for the uav aerial refueling problem. *IEEE Transactions on Sustems, Man, and Cybernetics*, 38(6):791–801.

McLain, T. W. and Beard, R. W. 2000. Trajectory planning for coordinated rendezvous of unmanned air vehicles. *Proceedings of the AIAA Guidance, Navigation, and Control Conference*, 4369:1–8.

Moon, T. K. and Sterling, W. C. 2000. *Mathematical Methods and Algorithms.* Prentice Hall.

Murray, R. 1996. Trajectory generation for a towed cable system using differential flatness. *13th Triennial World Congress of the International Federation of Automatic Control*, pages 395–400.

Nelson, D. R., Barber, D. B., and McLain, T. W. 2007. Vector field path following for miniature air vehicles. *IEEE Transactions on Robotics*, 23:519–529.

Simon, D. and Chia, T. L. 2002. Kalman filtering with state equality constraints. *IEEE Transactions on Aerospace and Electronic Systems*, 38(1):128–136.

Siouris, G. M. 2004. *Missile Guidance and Control Systems.* Springer-Verlag, New York.

Skjetne, R., Fossen, T., and Kokotovic, P. 2004. Robust output maneuvering for a class of nonlinear systems. *Automatica*, 40(3):373–383.

Skop, R. A. and Choo, Y. 1971. The configuration of a cable towed in a circular path. *Journal of Aircraft*, 8(11):856–862.

Turkyilmaz, Y. and Egeland, O. 2001. Active depth control of towed cables in 2d. *IEEE Conference on Decision and Control*, pages 952–957.

Udwadia, F. E. and Kalaba, R. E. 1996. *Analytical Dynamics: A New Approach.* Cambridge University Press.

Williams, P. and Ockels, W. 2009. Dynamics of towed payload system using multiple fixed-wing aircraft. *Journal of Guidance, Control, and Dynamics*, 32(6):1766–1780.

Williams, P., Sgarioto, D., and Trivailo, P. M. 2008. Constrained path-planning for an aerial-towed cable system. *Aerospace Science and Technology*, 12:347–354.

Williams, P. and Trivailo, P. 2007a. Dynamics of circularly towed cable systems, part 1: Optimal configurations and their stability. *AIAA Journal of Guidance Control and Dynamics*, 30(3):753–765.

Williams, P. and Trivailo, P. 2007b. Dynamics of circularly towed cable systems, part 2: Transitional flight and deployment control. *AIAA Journal of Guidance Control and Dynamics*, 30(3):766–779.

Yang, C. and Blasck, E. 2006. Kalman filtering with nonlinear state constraints. In *2006 9th International Conference on Information Fusion*.

Zarchan, P. 1990. *Tactical and Strategic Missile Guidance*, volume 124 of *Progress in Astronautics and Aeronautics*. American Institute of Aeronautics and Astronautics, Washington DC.